Polarity of Chemical Bonds via Hyperpolarizabilities. Determination of the Direction of the P–H Bond Dipole of LiH_2PO_3 from Measurements of Nonlinear Optical Coefficients

J. G. Bergman,*[1a] A. P. Ginsberg,*[1b] and M. Maurin[1c]

Contribution from Bell Laboratories, Holmdel, New Jersey 07733, Bell Laboratories, Murray Hill, New Jersey 07974, and the Laboratoire des Acides Mineraux, Université des Sciences et Techniques du Languedoc, Montpellier, France. *Received June 28, 1979*

Abstract: The direction of a bond dipole in a charged complex can be determined from measurements of nonlinear optical coefficients of a crystal containing the complex. As an example, optical second harmonic generation measurements on single crystals of LiH_2PO_3 lead to the conclusion that the P–H bond dipole direction is $P^{\delta+}$–$H^{\delta-}$. The same conclusion is reached by a molecular orbital analysis (SCF-Xα-SW method) on HPO_3^{2-}. The MO results are also of interest in that they contradict the often-made assumption that the hyperpolarizability and polarizability of a molecule are due almost entirely to charge in the bonding region between atoms.

Introduction

Polarity of chemical bonds, as measured by bond dipole moments, has been of longstanding interest.[2a] The experimental origins of bond dipole values are molecular dipole moments which may be expressed as vector sums of the bond dipoles. Because the usual methods of measuring dipole moments cannot be applied to charged species, there has been no experimental method for determining the polarity of a bond in an ionic complex. In this paper we point out that it is possible to determine the direction of a bond dipole in a complex ion from measurements of the nonlinear optical coefficients of a crystal containing the ion.

The dipole moment **P** induced in a molecular system by an electromagnetic field of strength E is given in terms of the field strength by

$$\mathbf{P} = \alpha E + \beta E^2 + \gamma E^3 \qquad (1)$$

where α is the linear polarizability of the system and β and γ are called the first and second hyperpolarizabilities, respectively.[2b] We will be concerned with the first hyperpolarizability, a third-rank tensor which has nonzero components only in systems with a permanent dipole moment. β is related to individual bond polarities by making the assumption (bond additivity approximation[2b]) that its components can be expressed as a sum of individual bond hyperpolarizabilities β_b. β for a molecule with N bonds is then written as

$$\beta_{ijk} = \sum_{b=1}^{N} (\beta_b)_{ijk} \qquad (2)$$

where i, j, and k denote Cartesian coordinates. If we make the further assumption that a chemical bond has approximate $C_{\infty v}$ symmetry, β_b will be completely specified by its components parallel ($\beta^{\parallel}{}_b$) and perpendicular ($\beta^{\perp}{}_b$) to the bond axis; all other components of β_b will be zero in a coordinate system with z axis along the bond dipole.[3-5] For our purposes, the important point to note about β_b is that the sign of both $\beta^{\parallel}{}_b$ and $\beta^{\perp}{}_b$ is determined by the orientation (parallel or antiparallel) of the permanent bond dipole with respect to the external field along the bond axis.[2b] A determination of the sign of $\beta^{\parallel}{}_b$ or $\beta^{\perp}{}_b$ for two different bonds (in the same or different molecules) therefore gives the relative orientation of the two bond dipoles.

Bond hyperpolarizabilities for a complex ion may be determined from an optical second harmonic generation experiment on an acentric crystal containing the ion. This experiment measures the nonlinear optical coefficients d_{ijk} which are related to β_b by[3-5]

$$d_{ijk} = V^{-1} \sum_b \{\gamma_i\gamma_j\gamma_k(\beta^{\parallel}{}_b - 3\beta^{\perp}{}_b) + (\gamma_i\delta_{jk} + \gamma_j\delta_{ki} + \gamma_k\delta_{ij})\beta^{\perp}\} \qquad (3)$$

where γ_i is the ith direction cosine of bond b, δ_{ij} is the Kronecker δ function, and the summation is over all bonds in the unit cell of volume V. The prerequisites for using eq 3 to determine bond polarities in a complex ion are: (1) The complex must be acentric and must be available in an acentric crystal lattice. (2) The complete crystal structure must be known. (3) The crystals must be optically transparent and capable of being prepared with optically flat surfaces.[5]

As a demonstration of the method, we have determined the direction of the P–H bond dipole in the anion $[HPO_2OH]^-$ in the salt LiH_2PO_3. This material meets the requirements mentioned above and has the advantage that, in addition to the P–H bond, it contains a dipole of presumably known direction ($P^{\delta+}$–$O^{\delta-}$); a separate optical interference experiment with a reference crystal is therefore unnecessary. The experimentally determined P–H dipole direction is $P^{\delta+}$–$H^{\delta-}$.

In order to appraise the validity of our result we have carried out a molecular orbital analysis of HPO_3^{2-} using the self-consistent-field Xα scattered wave (SCF-Xα-SW) method.[6-8] The calculated charge distribution is in agreement with the experimental P–H dipole direction. In addition, the calculations provide a description of the bonding character of the electrons which contribute to the polarizability and the hyperpolarizability of HPO_3^{2-}. It is clear from these results that, contrary to a frequently made assumption, nonbonding electrons can make important contributions to the hyperpolarizability of a molecule.

Experimental Section

Water white crystals (~5 mm on a side) of LiH_2PO_3 were grown from an aqueous solution by evaporation. The indices of refraction, shown in Table I, were obtained from a combination of conoscopic and index matching oil observations as well as birefringence and coherence length measurements. Table I also lists the literature values for the crystallographic parameters of LiH_2PO_3.[9]

Neglecting dispersion in d_{ijk}, the five independent nonlinear optical coefficients subject to symmetry $mm2$ are reduced to three, viz., d_{333}, $d_{311} = d_{113}$, and $d_{322} = d_{223}$. These coefficients, shown in Table II

0002-7863/80/1502-0118$01.00/0

Table I. Indices of Refraction[a] and Cell Constants[b] of LiH_2PO_3

symmetry	$Pna2_1$	
a_0	11.0 Å	
b_0	5.06 Å	
c_0	5.17 Å	
	1.06 μ	0.53 μ
n_a	1.560	1.575
n_b	1.571	1.590
n_c	1.555	1.570

[a] Absolute values of the indices are probably accurate to ±2%. [b] From ref 9b.

Table II. Nonlinear Coefficients (d_{ijk}'s) and Coherence Lengths (l_{ij}'s) for LiH_2PO_3[a]

ijk	$\lvert d_{ijk}\rvert$ (×10^{-9}), esu
333	1.6
311	0.61
113	0.62
322	0.11
223	0.13
	$d_{333} \times d_{311} < 0$
ij	l_{ij}, μ
33	+18
31	+27.3
15	±15.5
32	±200
24	±16

[a] Absolute values of (d,l) are ±(20, 5%) respectively. Coefficients were measured relative to quartz and converted to absolute units via $d^0_{111} = 1.2 \times 10^{-9}$ esu.

along with their respective coherence lengths, were measured on wedge-shaped samples using a Q-switched Nd-YAG laser operating at 1.06 μ. Details of the experimental setup are given elsewhere.[3-5]

Experimental Results

Using the structural parameters of Johansson and Lindquist and the results of Table II, we obtain the following three equations from eq 3:

$$0.85\beta^{\parallel}_{PO} - 1.31\beta^{\perp}_{PO} - 0.03\beta^{\parallel}_{PH} - 0.87\beta^{\perp}_{PH} = 1.14 \times 10^{-31} \text{ esu} \quad (4)$$

$$-0.19\beta^{\parallel}_{PO} + 0.98\beta^{\perp}_{PO} - 0.28\beta^{\parallel}_{PH} + 0.51\beta^{\perp}_{PH} = -0.43 \times 10^{-31} \text{ esu} \quad (5)$$

$$-0.25\beta^{\parallel}_{PO} + 1.16\beta^{\perp}_{PO} - 0.01\beta^{\parallel}_{PH} - 0.29\beta^{\perp}_{PH} = \pm 0.09 \times 10^{-31} \text{ esu} \quad (6)$$

The sign of the right-hand side of eq 6 is uncertain because the magnitude of d_{322} was too small for its sign to be determined. In deriving eq 4-6 the contribution of the O-H bond to the hyperpolarizability of $[HPO_2OH]^-$ was not explicitly included. From eq 4-6 we find

$$\beta^{\parallel}_{PH} = 1.25\beta^{\parallel}_{PO} - 0.92 \times 10^{-31} \quad (7a)$$

or

$$\beta^{\parallel}_{PH} = 1.25\beta^{\parallel}_{PO} - 0.98 \times 10^{-31} \quad (7b)$$

and

$$\beta^{\perp}_{PH} = 1.28\beta^{\perp}_{PO} - 0.77 \times 10^{-31} \quad (8a)$$

or

$$\beta^{\perp}_{PH} = 1.28\beta^{\perp}_{PO} - 0.45 \times 10^{-31} \quad (8b)$$

The alternate forms of eq 7 and 8 depend upon the sign chosen for eq 6. From eq 7 it is evident that, if $\beta^{\parallel}_{PO} > 0$, $\beta^{\parallel}_{PH} > 0$ so long as $\beta^{\parallel}_{PO} > 0.74 \times 10^{-31}$, while, if $\beta^{\parallel}_{PO} < 0$, $\beta^{\parallel}_{PH} < 0$ always. From the literature, $\beta^{\parallel}_{PO} = 11.4 \times 10^{-31}$ esu in PO_4.[3,4] Although $\beta^{\parallel}_{PO}$ in $[HPO_2OH]^-$ may be substantially different from the value in PO_4^{3-}, it cannot have decreased by more than an order of magnitude. We therefore conclude that $\beta^{\parallel}_{PH}$ has the same sign as $\beta^{\parallel}_{PO}$, i.e., that the dipole direction is $P^{\delta+}$-$H^{\delta-}$. A similar argument for $\beta^{\perp}_{PH}$ is unnecessary since it must have the same sign as $\beta^{\perp}_{PH}$.

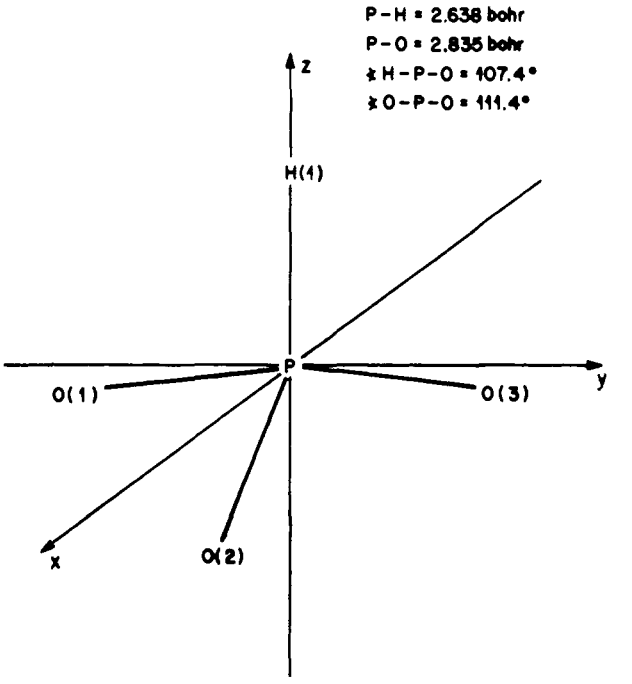

Figure 1. Coordinate system, geometry, and labeling scheme for HPO_3^{2-} (C_{3v}).

Table III. Atomic Coordinates, Exchange Parameters, and Sphere Radii for HPO_3^{2-} (au)[a]

	X	Y	Z	α	R
P	0	0	0	0.726 20	1.844
H	0	0	2.638	0.777 25	1.454
O(1)	−1.353	−2.343	−0.848	0.744 47	1.700
O(2)	2.705	0	−0.848	0.744 47	1.700
O(3)	−1.353	2.343	−0.848	0.744 47	1.700
OUT	0	0	−0.526	0.746 20	4.424
INT				0.742 03	

[a] 1 bohr = 0.529 17 Å. OUT refers to the outer sphere surrounding the entire cluster, and INT refers to the regions between the atomic spheres and inside the outer sphere.

Procedure for Molecular Orbital Calculations

SCF-Xα-SW calculations were carried out in double precision on Honeywell 6000 and IBM 370/168 computers using current versions of the programs written originally by K. H. Johnson and F. C. Smith. Orbital dipole moments were calculated from the Xα wave functions by the method of Case and Karplus[3] using the program by D. A. Case.

Figure 1 shows the coordinate axes and geometry used in the calculation; HPO_3^{2-} was assumed to have C_{3v} symmetry. The bond distances and angles in Figure 1 are averages of the values found for LiH_2PO_3 by neutron diffraction.[9b] Atomic coordinates for the calculation were derived from the structural parameters in Figure 1 and are summarized in Table III. Also given in Table III are the α exchange-correlation parameters and sphere radii used in the calculation. The α value for hy-

Table IV. Ground State Valence and Core Energy Levels, Charge Distributions, and Orbital Descriptions for HPO_3^{2-}

level[a]	energy, Ry	charge distribution, %[b]					major spherical harmonic[c]			description[d]
		P	H	3O	INT	OUT	P	H	O	
6e	−0.620	1	0	71	27	1			p	O nonbonding
$8a_1$	−0.638	6	17	55	17	4		s	p_z	O,H nonbonding
5e	−0.672	4	0	72	22	1			p	O nonbonding
$1a_2$	−0.698	0	0	66	33	0			p	O nonbonding
$7a_1$	−0.751	15	5	58	18	3	p_z, s		p	P–O σ bonding
4e	−0.772	16	0	58	25	1	$p_{x,y}$		p	P–O σ bonding
$6a_1$	−1.063	30	27	22	17	3	s, p_z	s	p, s	P–H σ bonding
3e	−1.719	3	0	85	11	0			s	O nonbonding
$5a_1$	−1.949	21	0	71	7	1	s		s	P–O σ bonding
P2p core	−9.537	100	0	0	0	0				
P2s core	−13.079	100	0	0	0	0				
O1s core	−37.514	0	0	100	0	0				
P1s core	−153.047	100	0	0	0	0				

[a] Only the occupied levels are given. [b] Percentage of the total population of the level located within the indicated regions, 3O refers to the combined oxygen spheres. [c] Spherical harmonic basis functions contributing more than 10% of the charge in regions containing more than 10% of the population of the level. [d] The principal characteristic of the orbital; the nonbonding orbitals also have weak bonding character.

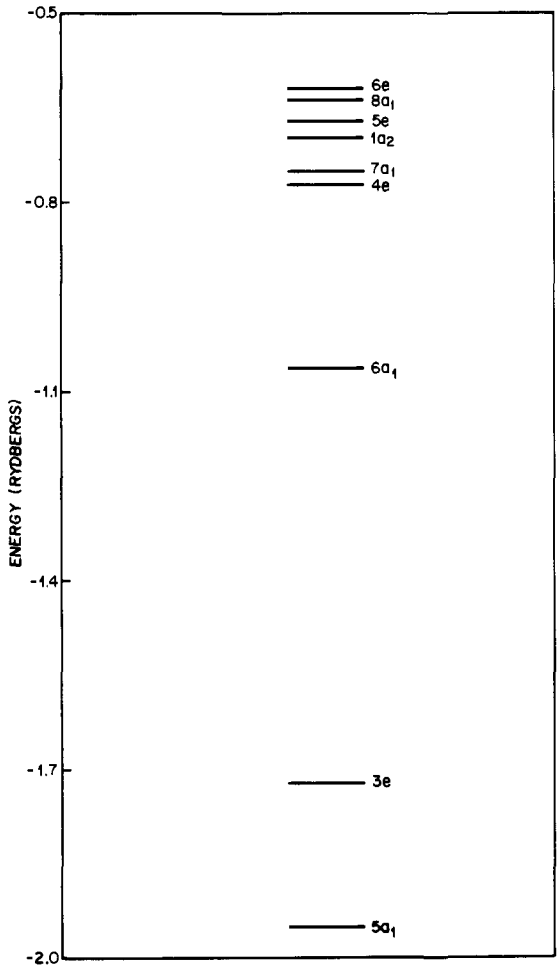

Figure 2. SCF ground-state one-electron valence energy levels for HPO_3^{2-}

drogen is that recommended by Slater;[11] the values for phosphorus and oxygen are from Schwarz's table.[12] In the intersphere region α was taken to be a valence electron weighted average of α_H, α_P, and α_O. A similarly weighted average of α_H and α_O was used in the extramolecular region. Overlapping atomic sphere radii were obtained by increasing the radii of touching atomic number spheres[13] by 25%[14] without attempting optimization with respect to the virial ratio. The outer sphere was taken to be tangent to the oxygen spheres and was centered at the valence electron weighted average of the atom

Table V. Orbital Dipole Moment Contributions[a]

orbital	dipole, au		
	X	*Y*	*Z*
6e	0.1	0.0	−3.4
$8a_1$	0.0	0.0	0.2
5e	0.1	0.0	−3.2
$1a_2$	0.0	0.0	−1.7
$7a_1$	0.0	0.0	−1.0
4e	−0.1	−0.1	−2.8
$6a_1$	0.0	0.0	2.0
3e	0.2	0.1	−3.2
$5a_1$	0.0	0.0	−1.3

[a] The calculated total electronic dipole moment in the *Z* direction is −49.28 D. The total net dipole (electronic + nuclear) is −4.25 D.

Table VI. Ground-State Total Energies (Ry) and Total Charge Distribution for HPO_3^{2-}

total energy	−1131.6424
kinetic energy (*T*)	1136.1025
potential energy (*V*)	−2267.7449
$-2T/V$	1.0020
Total Charge in the Different Regions (e^-)	
P	12.390
H	1.008
O1	7.636
O2	7.636
O3	7.636
extramolecular	0.394
intersphere	5.298

positions. A Watson sphere,[15] concentric with the outer sphere and bearing a +2 charge, was used to simulate the electrostatic interaction of the cluster with its surrounding crystal lattice.

The initial cluster potential for HPO_3^{2-} was obtained by superposition of SCF-Xα charge densities for P^0, H^0, and $O^{-0.666}$. Partial waves through $l = 3$ in the extramolecular region, $l = 2$ in the phosphorus sphere, $l = 1$ in the oxygen spheres, and $l = 0$ in the hydrogen sphere were used to expand the wave functions. C_{3v} symmetry was used to factor the secular matrix. The ground-state one-electron eigenvalues were converged to ±0.0009 Ry or better for the valence levels and to better than ±0.002 Ry for the core levels; a 9:1 average of the initial and final potential for a given iteration was used as the starting potential for the next iteration. Core levels were not frozen at any point in the calculation.

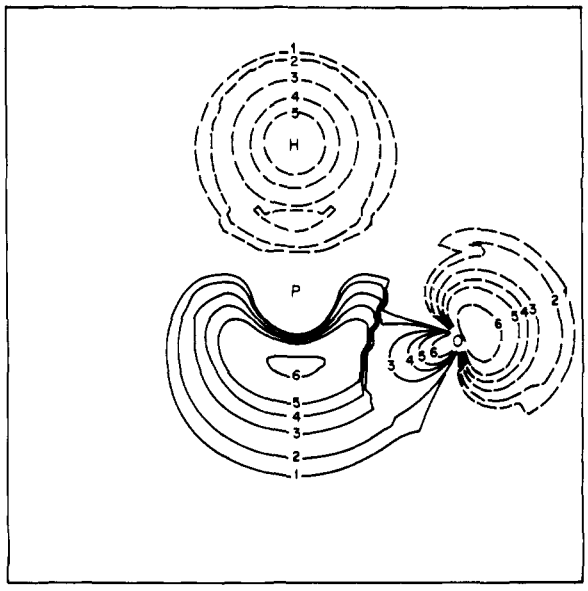

Figure 3. Wave function contour map of the $7a_1$ orbital in the xz plane. The contour values are ±1, ±2, ±3, ±4, ±5, ±6 = ±0.04, ±0.06, ±0.08, ±0.10, ±0.15, ±0.20 (electrons/bohr^3)$^{1/2}$.

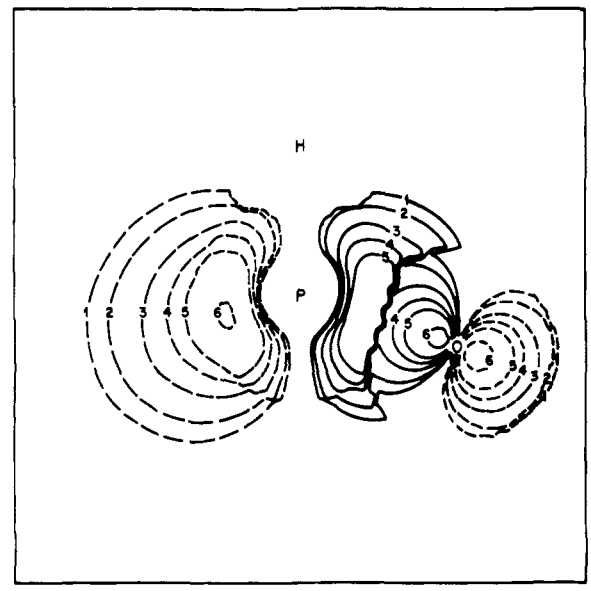

Figure 4. Contour map of one of the two degenerate 4e wave functions in the xz plane. Contour values as in Figure 3.

Results of Molecular Orbital Calculations

The calculated ground-state one-electron energies, charge distributions, and orbital descriptions for HPO_3^{2-} are given in Table IV. Figure 2 is a diagram of the valence energy levels. Wave function contour maps of selected orbitals are shown in Figures 3 and 4. These maps were each generated from the numerical values of the wave function at 6561 grid points within a 10 × 10 (bohr)^2 area centered on the origin. The calculated dipole moment contributions for the different orbitals are summarized in Table V. Table VI gives the ground-state total energies and total charge distribution. To obtain net atomic charges from the total charge distribution in Table VI, it is necessary to partition the charge in the intersphere and extramolecular regions among the atomic spheres. Table VII gives the net charges for two partitioning methods. In method (A) the intersphere charge is distributed between the H, P, and O spheres in proportion to the number of valence electrons on the neutral free atoms while the extramolecular charge is similarly distributed between the H and O spheres. In method (B), the intersphere charge is distributed according to the Case and Karplus procedure,[10] while the extramolecular charge is distributed as in method (A).

Table VII. Net Atomic Charges in HPO_3^{2-}

atom	method A[a]	method B[a]
P	+1.62	+1.71
H	−0.37	−0.33
O	−1.08	−1.12

[a] Method A and method B refer to different ways of distributing the intersphere and extramolecular charge between the atomic spheres. See text for explanation.

Discussion

From the dipole moments in Table V and from the net atomic charges in Table VII, it is seen that the Xα-SW analysis predicts the dipole directions to be $P^{\delta+}$-$O^{\delta-}$ and $P^{\delta+}$-$H^{\delta-}$, in agreement with the result of the second harmonic generation experiment.

Examination of Table IV and Figure 2 shows that four nonbonding oxygen orbitals, spread over a range of 0.08 Ry, are the highest occupied levels of HPO_3^{2-}. Electrons in these orbitals are presumably the most polarizable in the molecule, and the three levels in this group which also have large dipole moments (6e, 5e, and $1a_2$; compare Table V) are expected to make important contributions to the nonlinear susceptibility. At 0.05–0.07 Ry below the nonbonding $1a_2$ level are the P–O bonding $7a_1$ and 4e levels; electrons in these orbitals are also expected to contribute significantly to the nonlinear susceptibility. The P–H bonding orbital, $6a_1$, is 0.3 Ry below the 4e level. P–H bonding electrons will therefore be much less polarizable than the higher energy nonbonding and P–O bonding electrons and will be less important in contributing to the nonlinear susceptibility. Electrons in the much deeper 3e and 5a orbitals will make even less contribution to the nonlinear susceptibility.

It is interesting to compare the above conclusions about the nature of the electrons contributing to the nonlinear susceptibility with the common assumption (e.g., in the bond charge model[16]) that the susceptibility (nonlinear and linear) is due almost entirely to charge in the bonding region between atoms. The detailed calculations on HPO_3^{2-} contradict this assumption in two respects. First, as we have already seen, the nonbonding electrons can make a major contribution. Furthermore, examination of contour diagrams such as Figures 3 and 4 for orbitals expected to make important contributions to the nonlinear susceptibility shows the presence of polarizable charge outside of the bonding region, even for bonding orbitals. Our analysis also makes it clear that so-called bond polarizabilities and hyperpolarizabilities based on the bond additivity approximation may contain contributions from nonbonding electrons.[17]

References and Notes

(1) (a) Bell Laboratories, Holmdel, N.J.; (b) Bell Laboratories, Murray Hill, N.J.; (c) Université des Sciences et Techniques du Languedoc.
(2) (a) See, for example, C. P. Smyth, "Dielectric Behavior and Structure", McGraw-Hill, New York, 1955, Chapters 8–13. (b) A. D. Buckingham and B. J. Orr, *Q. Rev., Chem. Soc.*, **21**, 195 (1967).
(3) J. G. Bergman and G. R. Crane, *J. Chem. Phys.* **60**, 2470 (1974).
(4) J. G. Bergman and G. R. Crane, *J. Solid State Chem.*, **12**, 172 (1975).
(5) G. R. Crane and J. G. Bergman, *Inorg. Chem.*, **17**, 1613 (1978).
(6) K. H. Johnson, *Annu. Rev. Phys. Chem.*, **26**, 39 (1975).
(7) J. C. Slater, "The Self-Consistent Field for Molecules and Solids: Quantum Theory of Molecules and Solids", Vol. 4, McGraw-Hill, New York, 1974.
(8) J. C. Slater, "The Calculation of Molecular Orbitals", Wiley, New York, 1979.
(9) (a) E. Philippot and O. Lindqvist, *Acta Chem. Scand.*, **25**, 2803 (1970); (b) G. B. Johansson and O. Lindqvist, *Acta Crystallogr., Sect. B*, **32**, 412 (1976).
(10) D. A. Case and M. Karplus, *Chem. Phys. Lett.*, **39**, 33 (1976).

(11) J. C. Slater, *Int. J. Quantum Chem., Suppl.*, **7**, 533 (1973).
(12) K. Schwarz, *Phys. Rev. B*, **5**, 2466 (1972).
(13) J. G. Norman, Jr., *Mol. Phys.*, **31**, 1191 (1976).
(14) D. R. Salahub, R. P. Messmer, and K. H. Johnson, *Mol. Phys.*, **31**, 529 (1976).
(15) R. E. Watson, *Phys. Rev.*, **111**, 1108 (1958).
(16) B. F. Levine, *Phys. Rev., B*, **7**, 2600 (1973). Although the bond charge model explicitly assumes the predominant importance of the charge in the bonding region, Levine has pointed out to us that the model in fact indirectly includes the effect of nonbonding charge since it uses linear susceptibilities to determine unknown parameters. This is probably an important reason for the success of the model.
(17) The bond additivity approximation, used in analyzing the experimental data, is independent of the bond charge model.

Spin Inversion in Triplet Diels–Alder Reactions

Sason S. Shaik*[†1a] and Nicolaos D. Epiotis*[1b]

Contribution from the Department of Chemistry, Cornell University, Ithaca, New York 14853, and the Department of Chemistry, University of Washington, Seattle, Washington 98195. *Received March 30, 1979*

Abstract: *Spin inversion in triplet* $[_\pi 4_s + _\pi 2_s]$ *complexes can be induced by stereochemically different mechanisms.* Consequently, triplet Diels–Alder reactions can be 4s + 2s stereospecific, 4s + 2a (4a + 2s) stereospecific, or stereorandom. The selection of one mechanism depends on the donor–acceptor relationship and the triplet energies of the reactants. It is predicted that enhancing the donor–acceptor relationship of the reactants, i.e., *increasing the reaction polarity*, will increase 4s + 2s product formation relative to all other products. On the other hand, decreasing the triplet energies, at constant polarity, will result in predominant 4s + 2a product formation. Solvent polarity will have a more pronounced effect on the yield of 4s + 2s adducts. The competition of [4 + 2] and [2 + 2] cycloaddition is discussed. It is predicted that the [4 + 2]/[2 + 2] product ratio will increase as polarity increases and it will decrease as the triplet energy of one or both reaction partners decreases.

Introduction

Photosensitized cycloadditions of dienes and olefins commonly result in a mixture of [2 + 2] and [4 + 2] adducts.[2,3] This nontoposelectivity[4a] is usually regarded as a result of formation of triplet diradical in the early stages of the photoreaction. It is assumed that the triplet diradical then inverts spin to yield a singlet diradical (not necessarily an intermediate) which subsequently may cyclize, giving rise to a mixture of [2 + 2] and [4 + 2] cycloadducts. This sequence of events is described schematically below.[2,3,4b]

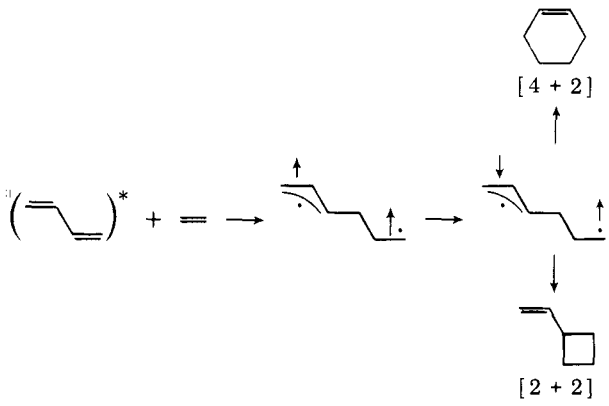

Interestingly, however, there are cases where the [4 + 2] adduct is the *only* product and others in which it is the *major* product of the cycloaddition.[3b] A typical example from the work of Schenck et al.[3b] is given below. In addition, an increase

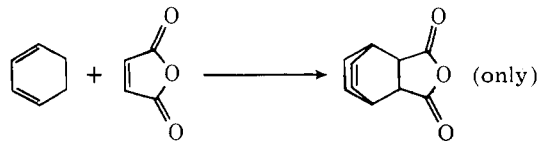

of the [4 + 2]/[2 + 2] cycloadducts ratio roughly follows an increase in *reaction polarity, defined as the inverse of* $I_D - A_A$, where I_D is the ionization potential of the donor and A_A is the electron affinity of the acceptor.

Reformulating the experimental trends: it seems that triplet Diels–Alder reactions can indeed be efficient. This behavior, which is not compatible with orbital-symmetry predictions for singlet photoreactions, is a reminder of trends observed in thermal reactivity.[5] It suggests the importance of yet another factor which is polarity dependent and that can differentiate between [2 + 2] and [4 + 2] cycloadduct formation.

Recently,[6] we have derived spin inversion mechanisms for $[_\pi 2_s + _\pi 2_s]$ triplet complexes.[7,8] There are several such mechanisms and each may lead to a stereochemically unique product. The relative efficiency of the mechanisms depends on reaction polarity and on the triplet energies of either reactant.[6c] Thus, we are able to understand the occurrence of stereospecific results in some polar $2\pi + 2\pi$ triplet cycloadditions.[9]

Let us now apply these ideas to $[_\pi 2_s + _\pi 4_s]$ triplet complexes. We will assume a certain reaction coordinate and find the spin inversion pathways resulting from it. Then we shall derive the dependence of these pathways on reaction polarity and on the triplet energies of the reactants, and compare the conclusions with available experimental data.

I. Theory

Since the theoretical background is described elsewhere[6] only a brief summary is given here. The efficiency of spin inversion depends on the spin–orbit (SO) coupling interaction of the triplet state, T_1, with the ground state, S_0. The interaction is proportional to the SO coupling matrix element, $\langle T_1|\hat{H}_{SO}|S_0\rangle$, and inversely proportional to the energy gap separating the two states.[10] Consequently, *efficient spin inversion can be induced by motions,* Q_k, *which maximize the SO coupling matrix element and minimize the* T_1–S_0 *separation.* In order to search for such motions we utilize a strategy which is explained in a previous paper.[6c] We use group theory to search for potentially efficient spin inversion motions (Q_k), on the basis of the equation

$$\Gamma(Q_k) = \Gamma(T_1^v) \times \Gamma(R_k) \times \Gamma(S_0) \qquad (k = x, y, z) \quad (1)$$

[†] Department of Chemistry, Ben-Gurion University, Beer Sheva 84120, Israel.

0002-7863/80/1502-0122$01.00/0